





Tuning superconductivity and charge density wave order in TaSe₂ through Pt intercalationMukhtar Lawan Adam ^{1,2,*}, Ibrahim Buba Garba ^{3,4}, Abba Alhaji Bala ⁵, Abdulsalam Aji Suleiman ^{6,†}, Sulaiman Muhammad Gana,² and Faisal Lawan Adam²¹*Materials Interfaces Center, Shenzhen Institute of Advanced Technology, Chinese Academy of Sciences, Shenzhen 518055, Guangdong, People's Republic of China*²*Physics Department, Bayero University, Kano 700231, Nigeria*³*Sorbonne Université, CNRS, IMPMC, 4 Place Jussieu, Paris 75252, France*⁴*Department of Physics, Federal University Gashua, Gashua 671106, Nigeria*⁵*Physics Department, Federal University Dutse, Jigawa 720101, Nigeria*⁶*Institute of Materials Science and Nanotechnology, Bilkent University UNAM, Ankara 06800, Turkey* (Received 4 December 2022; revised 14 February 2023; accepted 1 March 2023; published 14 March 2023)

Tantalum diselenide (TaSe₂) has emerged as a promising platform to investigate the interplay between two intriguing quantum electronic states in materials: the charge density wave order (CDW) and superconductivity. In this work, we report the ability to tune these quantum electronic states by intercalating Pt into 2H-TaSe₂. By introducing 20% of Pt into 2H-TaSe₂, we demonstrate that the structural phase changes from the 2H to the 4H_b phase of TaSe₂ with Pt atoms intercalated within the van der Waals spacing. According to the Fermi surface of the 4H_b phase, a Lifshitz transition occurred, destroying the Fermi-surface nesting found in the 2H phase. This can be attributed to the structural phase transformation and the influence of donated electrons from Pt, thus tuning the Van Hove singularities into the Fermi-level vicinity, suppressing the CDW state, and enhancing the superconducting temperature (T_c) to ~ 2.7 K. The resulting superconducting properties of the 4H_b-Pt_{0.2}TaSe₂ are consistent with those of a BCS type-II superconductor, with a superconducting gap of 3.0 meV. Our results provide insights into the role of electron doping and structural phase changes in fine-tuning quantum electronic-state phenomena in materials. These findings could have significant implications in designing superconducting materials with tailored properties for practical applications.

DOI: [10.1103/PhysRevB.107.104510](https://doi.org/10.1103/PhysRevB.107.104510)**I. INTRODUCTION**

Materials cohosting charge density wave (CDW) and superconducting states have been the subject of intensive research in condensed matter physics and materials sciences, providing a unique platform to understand the interplay between these two fundamental electronic quantum states [1–10]. A route that can carefully assist in fine-tuning these states is essential in understanding the interplay. Recently, inducing structural phase transition and Van Hove singularities (VHs) tuning has been demonstrated to enhance quantum electronic states in materials [11–16]. Structural changes can influence the position of the VHs; when fine-tuned to the vicinity of the Fermi surface (FS) of materials, it is observed to be accompanied by the emergence of electronic instabilities [17–19]. These electronic instabilities at the FS vicinity introduce delocalized electrons into the “Fermi sea,” creating low-energy excitations, thus significantly impacting the overall electronic properties of materials [20–22]. This has led to the enhancement or formation of exotic quantum states such as superconductivity, ferromagnetism, and spin-density wave states in kagome metals, graphene, sulfur hydrides, and transition-metal dichalcogenides (TMDs)

[1,2,13,23–29]. Due to the emergence of these exotic phenomena, several routes, such as doping and pressure, have been exploited to fine-tune the VHs in materials into the FS vicinity [12,14,26,30,31]. The VHs appears as an electronic phenomenon forming a saddlelike feature in the electronic band structure [32,33]. At the VHs, the density of states (DOS) diverges logarithmically to form highly localized electronic states [30,34]. On tuning the VHs to the Fermi vicinity, the FS of materials undergoes a Lifshitz transition, modifying the electronic structure while preserving/breaking the structural symmetry [11,35,36].

Interestingly, some TMDs and kagome metals, amongst others, have exhibited the coexistence of CDW and superconductivity states with the VHs in their electronic band structures [1,2,5,21,37–39]. These quantum materials with VHs existing above/below the Fermi level can be tuned by electron/hole doping to fall within the as-desired position [23,31,40]. Here, we study bulk 2H-TaSe₂, cohosting superconductivity at $T_c \sim 0.1$ K and CDW order transition at ~ 110 K [41]. Furthermore, the VHs in the band structure lies around ~ 0.5 eV above the Fermi level along the K - G high-symmetry line [42]. Moreso, FS nesting in 2H-TaSe₂ has been attributed to forming CDW order [41]. Through doping or intercalation, TaSe₂ structural (from 2H to 1T, 4H_b, 3R, or 6R) and electronic phase transformation can be achieved [43]. Hence, taking advantage of these properties in 2H-TaSe₂, we will attempt to tune its quantum electronic properties.

*mladam.phy@buk.edu.ng

†abdulsalam@unam.bilkent.edu.tr

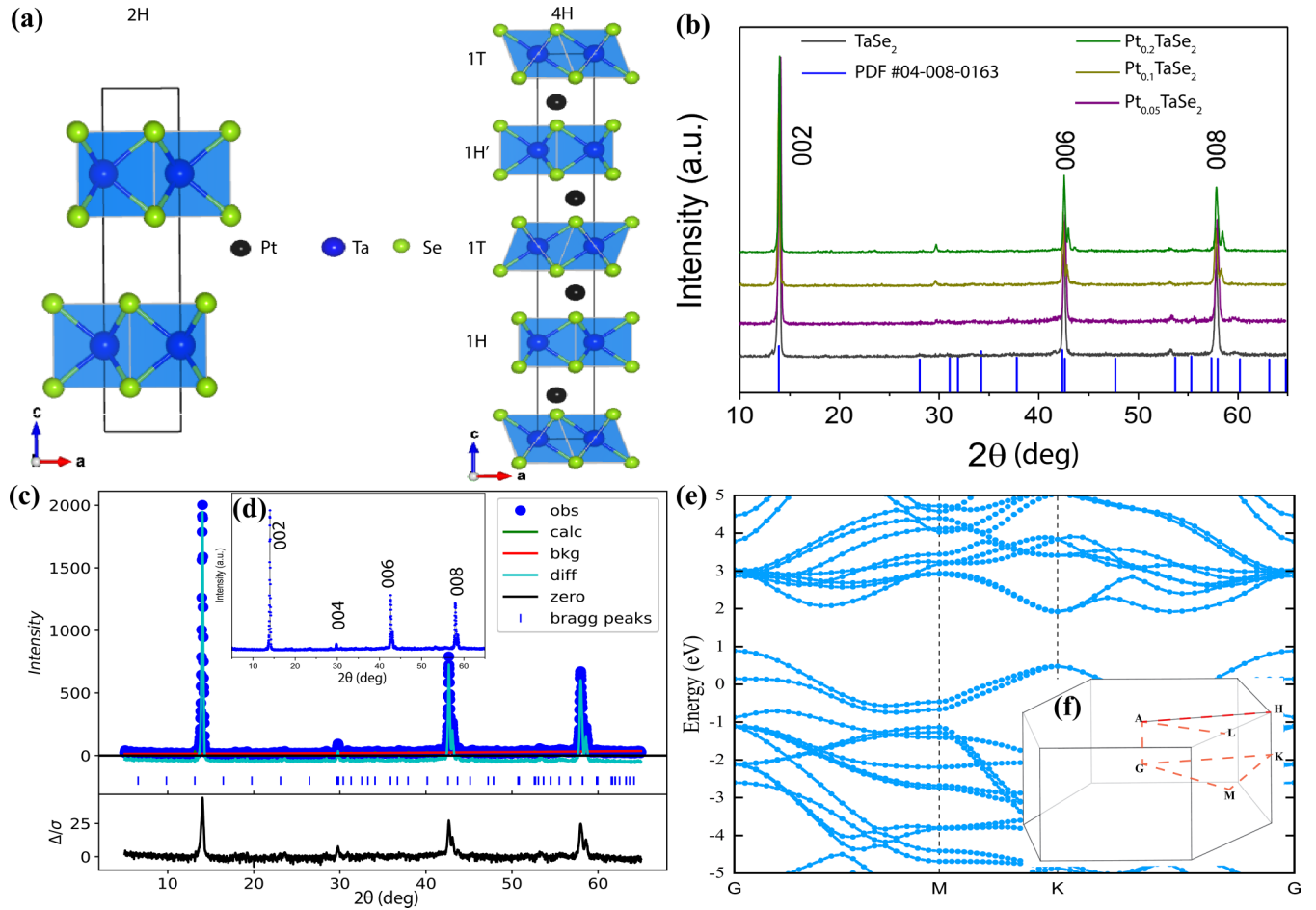


FIG. 1. (a) Side view of the crystal structure of $2H$ -TaSe₂ and Pt-intercalated $4H_b$ -TaSe₂. (b) XRD patterns of pristine $2H$ -TaSe₂ and Pt-doped TaSe₂. (c) XRD pattern and Rietveld refinement of $4H_b$ -Pt_{0.2}TaSe₂ at room temperature. Vertical (blue bars) stand for the positions of Bragg peaks. (d) Index XRD pattern of $4H_b$ -Pt_{0.2}TaSe₂. (e) Band structure of $2H$ -TaSe₂ (f) Brillouin zone indicating the high-symmetry points.

In this study, we modified the quantum electronic properties of $2H$ -TaSe₂ by carefully introducing electrons. These were achieved by intercalating Pt atoms into TaSe₂, as verified by x-ray photoelectron spectroscopy (XPS). However, at a concentration of 20% Pt, a structural phase transition occurs from a $2H$ to $4H_b$ phase, as confirmed through the Rietveld refinement of x-ray diffraction (XRD) data. Moreover, the VHS and Fermi surface tuning from the electronic structure can be observed to have occurred. This can be attributed to the occurrence of a Lifshitz transition. The resultant $4H_b$ -Pt_{0.2}TaSe₂ is found to be a type-II superconductor with a superconducting transition temperature of ~ 2.7 K and a completely suppressed CDW order.

II. EXPERIMENT AND DENSITY-FUNCTIONAL THEORY DETAILS

Single crystals of Pt_{*x*}TaSe₂ ($x = 0, 0.05, 0.1, \text{ and } 0.2$) were synthesized using the chemical vapor transport method. The stoichiometric molar ratio of high-purity Pt, Ta, and Se powders (purchased from Alfa Aesar and Sigma-Aldrich) were mixed based on Pt_{*x*}TaSe₂ ($x = 0, 0.05, 0.1, \text{ and } 0.2$) with one mole of iodine to serve as a transport agent, and the mixture

was then sealed in an air-evacuated ampoule tube. The sealed tubes were then placed at room temperature in a two-zone furnace and heated for 5 days while maintaining the furnace at 900 °C in the evaporation zone and 800 °C in the growth zone. The furnace was cooled to room temperature after 5 days. High-quality single crystals were obtained at the end of the ampoule. The crystal's diffraction was measured using a Panalytical x-ray diffractometer with $K\alpha$ radiation. Transport properties measurements at low temperatures were carried out using a Quantum Design physical property measurement system at the Hefei center for instruments, University of Science and Technology, China.

All first-principle calculations were carried out using the QUANTUM ESPRESSO [44] density-functional theory package to gain insight into the electronic properties of the compounds, with generalized gradient approximation of Perdew-Burke-Ernzerhof for the exchange correlation [45]. The cutoff energy of 90 Ry and a Gamma-centered k mesh of $11 \times 11 \times 5$ were used for the Brillouin-zone sampling. We also used the WANNI90 code [46] to obtain the materials' maximally localized functions; surface Green's function [47] was used as implemented in WANNIERTOOLS [46] package to calculate the surface states' dispersion of the materials.

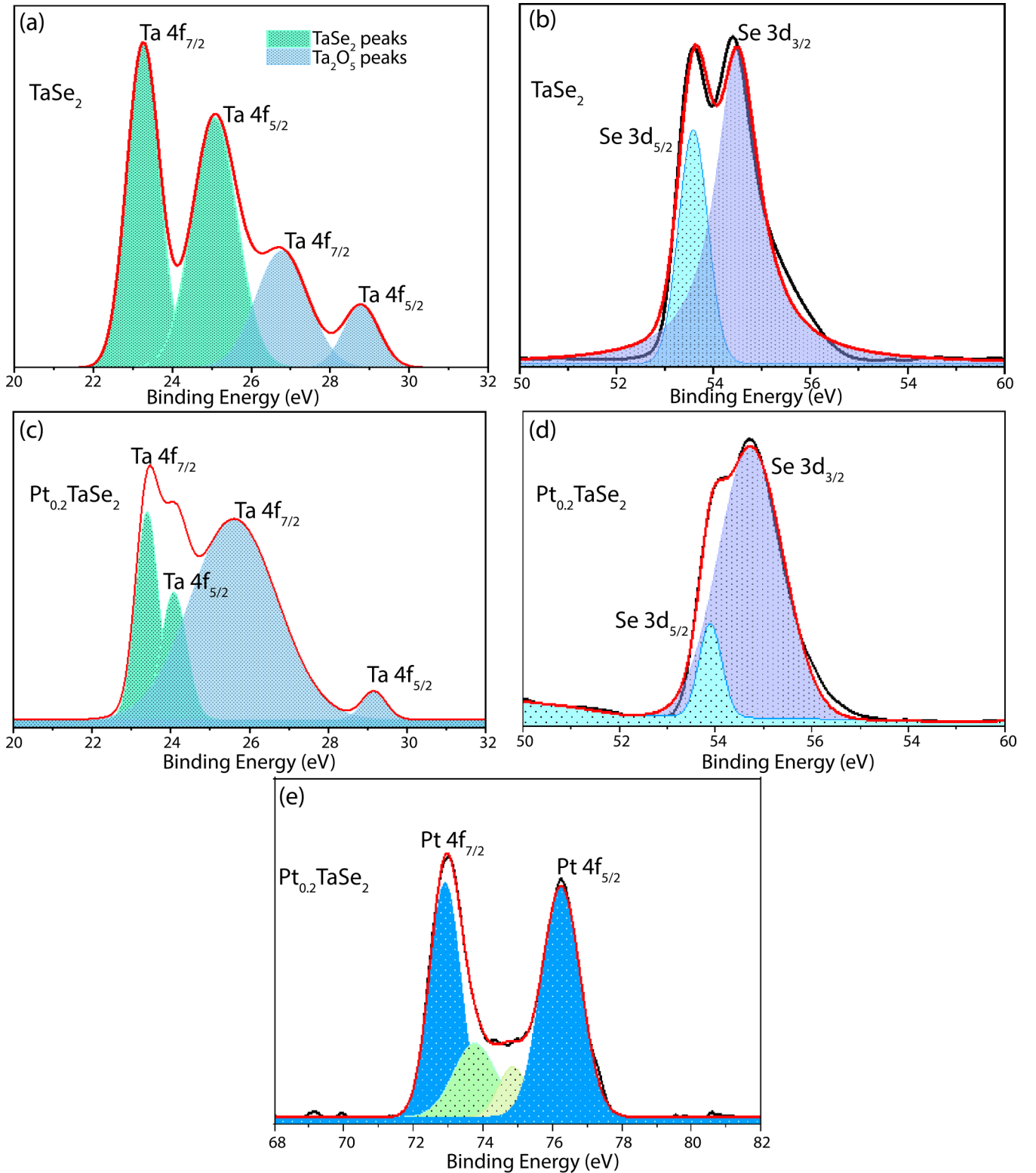


FIG. 2. XPS spectra of (a) Ta 4f region of $2H$ -TaSe₂. (b) Se 3d region of $2H$ -TaSe₂. (c) Ta 4f region of $4H_b$ -Pt_{0.2}TaSe₂. (d) Se 3d region of $4H_b$ -Pt_{0.2}TaSe₂. (e) Pt 4f region of $4H_b$ -Pt_{0.2}TaSe₂.

III. RESULTS AND DISCUSSION

Our extensive analysis, based on both experimental and theoretical results, reveals that the introduction of Pt atoms into TaSe₂ crystal introduces electron-like charge carriers.

The presence of such charge carriers in semimetal/metallic materials while hosting quantum electronic-states behavior such as CDW and superconductivity is known to modulate such states [37,38]. In our case, carrier doping in TaSe₂ suppressed the charge density wave states while enhancing the

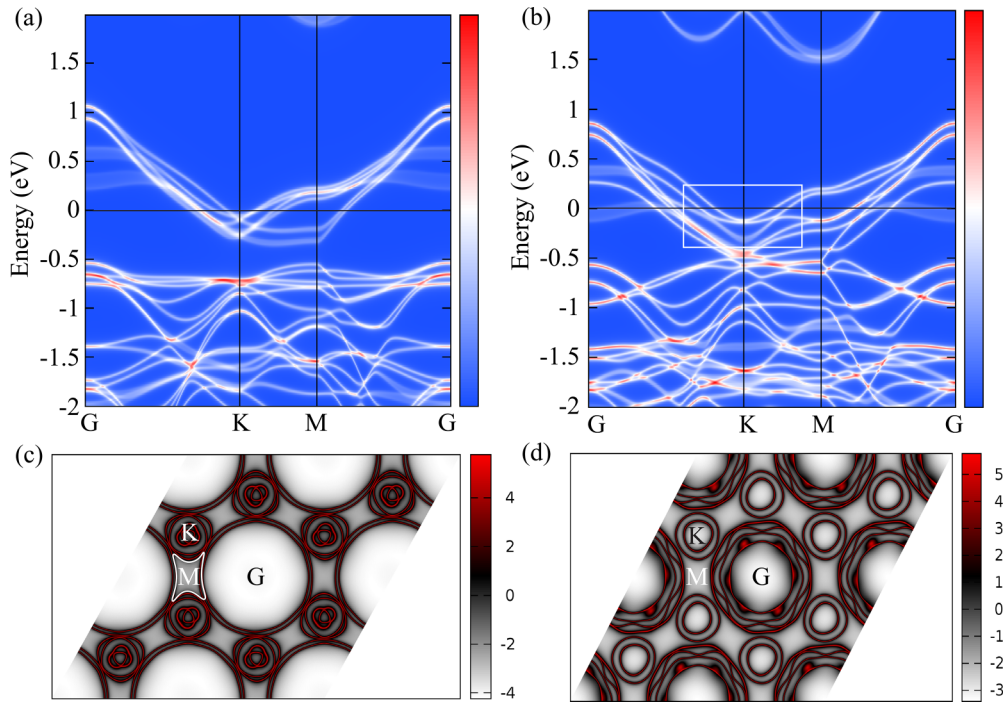


FIG. 3. Band structure of (a) $2H\text{-Pt}_{0.1}\text{TaSe}_2$ and (b) $4H_b\text{-Pt}_{0.2}\text{TaSe}_2$. Fermi surface of (c) $2H\text{-Pt}_{0.1}\text{TaSe}_2$ and (d) $4H_b\text{-Pt}_{0.2}\text{TaSe}_2$.

superconducting transition temperature, as demonstrated by transport properties measurement carried out at low temperatures.

Single crystals of the Pt_xTaSe_2 ($x = 0, 0.05, 0.1,$ and 0.2) compounds were synthesized using the chemical vapor transport method. The crystal structure of $2H\text{-TaSe}_2$ and the intercalated TaSe_2 with Pt atoms are visually represented in Fig. 1(a). X-ray diffraction was utilized to analyze the as-synthesized single crystals, as depicted in Fig. 1(b). The XRD results showed that $2H\text{-TaSe}_2$, $2H\text{-Pt}_{0.05}\text{TaSe}_2$, and $2H\text{-Pt}_{0.1}\text{TaSe}_2$ exhibit a hexagonal structure with a $P63/mmc$ space group, and the peaks were well indexed using the PDF No. 04-008-0163 card. A slight shift in the 002 peaks of $2H\text{-Pt}_{0.05}\text{TaSe}_2$ and $2H\text{-Pt}_{0.1}\text{TaSe}_2$ indicates possible lattice expansion. Also, possible new peaks were observed around $2\theta = 30^\circ$ and 53° in the XRD results of $\text{Pt}_{0.2}\text{TaSe}_2$. Rietveld refinements were performed on the XRD data of the sample using the GSAS-II software [48], with the results of the observed, calculated, and difference plots shown in Fig. 1(c) for $\text{Pt}_{0.2}\text{TaSe}_2$. The best fit was obtained when Pt atoms were placed in the octahedral positions of the van der Waals gaps between the TaSe_2 layers, forming a stacking sequence of $1H\text{-TaSe}_2$ and $1T\text{-TaSe}_2$ similar to the $4H_b\text{-TaSe}_2$ structure. The final agreement factors converged to $R_{\text{wp}} = 17.6\%$ with refined crystallographic data of $a = b = 3.476 \text{ \AA}$, $c = 26.917 \text{ \AA}$, $V = 281.755 \text{ \AA}^3$, and a $P63/mmc$ space group. All the indexed peaks of $4H_b\text{-Pt}_{0.2}\text{TaSe}_2$ are displayed in Fig. 1(d). Hence, it can be deduced that at doping 20% Pt into TaSe_2 , a crystal-structure phase modification from $2H$ to $4H_b$ occurs.

Building on our initial analysis, we utilized x-ray photoelectron spectroscopy to delve deeper into the behavior of Pt atoms in the as-synthesized compounds and to determine their chemical state. The XPS spectra of both the pristine and

the Pt-doped TaSe_2 are displayed in Fig. 2. On comparing the XPS spectra in Figs. 2(a)–2(d) of the Ta 4f and Se 3d region of both $2H\text{-TaSe}_2$ and $4H_b\text{-Pt}_{0.2}\text{TaSe}_2$, a subtle shift towards lower binding energy is observed in the latter. This suggests electrons transfer from Pt to the TaSe_2 host, leading to the formation of bonds with the Se atoms and a modification in the electronic structure of the materials. The presence of Ta_2O_5 peaks in Figs. 2(a) and 2(c) is attributed to oxides formation on the sample’s surface during post-treatment [49,50]. Furthermore, from the XPS spectra of $4H_b\text{-Pt}_{0.2}\text{TaSe}_2$ around the Pt 4f region, the Pt 4f_{7/2} peaks with a binding energy of 72.9 eV are in accord with Pt ions in the Pt^{2+} oxidation state [51,52], thus indicating a successful intercalation of Pt atoms into $2H\text{-TaSe}_2$.

Previous research has shown that electron/hole doping into the TaSe_2 can modify its intrinsic electronic properties [53–55]. The calculated bulk band structure of the $2H\text{-Pt}_{0.1}\text{TaSe}_2$ and $4H_b\text{-Pt}_{0.2}\text{TaSe}_2$, as shown in Fig. 3, was calculated using the WANNIER tool to easily distinguish between the compounds bulk and topological surface states, as well as the VFs features modulations. Neither of the compounds was observed to host nontrivial topological surface states from the bulk band structures in Figs. 3(a) and 3(b). However, there is significant modulation of the band structures of the compounds with the increase of Pt concentration from 10 to 20%. In comparison, as observed, the conduction bands show a downward shift.

One of the most critical observations in the Fermi surface map of CDW materials like $2H\text{-TaSe}_2$ is the presence of Fermi-surface nesting [54]. At the normal phase of $2H\text{-TaSe}_2$, its Fermi surface is known to host holelike pockets centered around G and K points, with “dog-bone”-shaped electron pockets around the M point [56,57] as shown in Fig. 3(c). However, at a commensurate CDW state with a

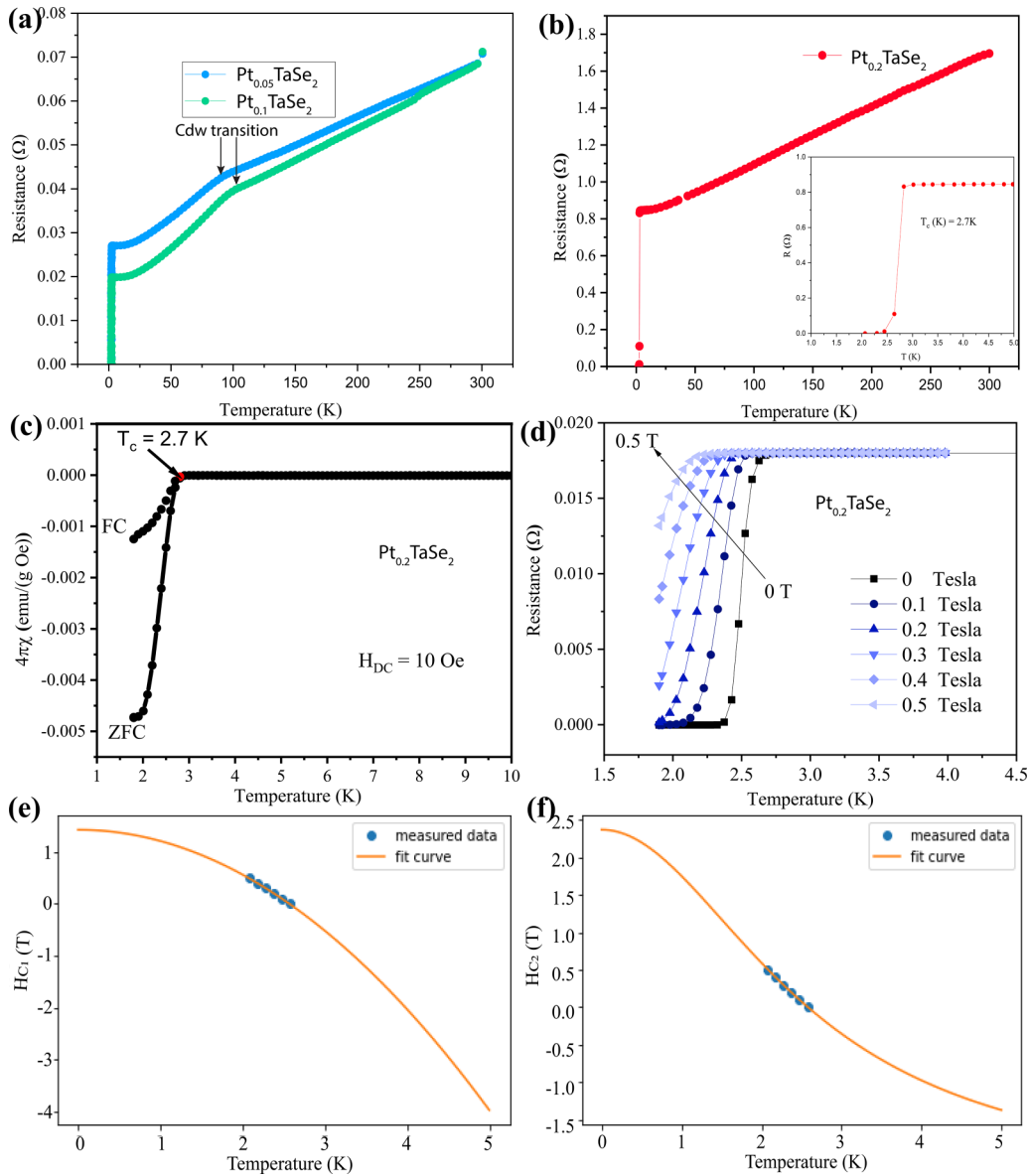


FIG. 4. (a) Plot of resistivity against the temperature of $2H$ - $\text{Pt}_{0.05}\text{TaSe}_2$ and $2H$ - $\text{Pt}_{0.1}\text{TaSe}_2$, indicating the charge density wave (CDW) transition. (b) Plot of resistivity against the temperature of $4H_b$ - $\text{Pt}_{0.2}\text{TaSe}_2$ (inset showing the superconducting transition temperature). (c) Measured zero-field-cooling (ZFC) and field-cooling (FC) magnetic susceptibility of $4H_b$ - $\text{Pt}_{0.2}\text{TaSe}_2$ under magnetic field $H_{DC} = 10$ Oe. (d) Resistivity against temperature plot under a varying magnetic field of $4H_b$ - $\text{Pt}_{0.2}\text{TaSe}_2$. (e) Plot of lower critical-field values against temperature. Orange line through the data is the best fit of the data to the Ginzburg-Landau equation with the $H_{c1} = 1.425$ T. (f) Plot of upper critical-field values against temperature. Orange line through the data is the best fit of the data to the WHH with the $H_{c2} = 2.367$ T.

3×3 state, the Fermi surface undergoes a reconstruction, and the dog bone around \mathbf{M} moves to the \mathbf{G} point, while the holelike pockets around the \mathbf{K} degenerate twice to form concentric pockets [39,53,56–59]. Figure 3(c) shows that from the Fermi-surface plots of $2H$ - $\text{Pt}_{0.1}\text{TaSe}_2$, there is almost an identical observation with the commensurate CDW Fermi surface of $2H$ - TaSe_2 , indicating a possible presence of a CDW state. However, at its \mathbf{K} point, electron-like pockets appear due to Pt doping.

Moreover, in an angle resolution photoelectron spectroscopy analysis of the CDW state suppression in Pd_xTaSe_2 [54], a topological Lifshitz transition is observed from electron-like pockets in the Fermi surfaces as observed in the $2H$ - TaSe_2 to two holelike pockets [60]. Accompanied by dis-

mantling the dog bone, Fermi surfaces are caused by the slight separation between the two holelike pockets. Interestingly, these two holelike pockets manifested a van Hove singularity of the saddle-point type, as observed in the Fermi-surface map.

As Fig. 3(d) shows, two degenerate holelike pockets appear at points \mathbf{K} and \mathbf{G} as the concentration of Pt increases from 10 to 20%. Moreover, these two holelike pockets corroborate with a saddle-point van Hove singularity feature, as seen in Fig. 3(b) around the \mathbf{K} high-symmetry point. Also, the dog bones, like the Fermi surface observed in $2H$ - $\text{Pt}_{0.1}\text{TaSe}_2$ around the \mathbf{M} point, are eliminated in $4H_b$ - $\text{Pt}_{0.2}\text{TaSe}_2$. Based on these findings, a change phase from a CDW material to a metal in $4H_b$ - $\text{Pt}_{0.2}\text{TaSe}_2$ can be said to have occurred.

The appearance of saddle-point VHS close to the Fermi level in materials amplifies the electron correlation, resulting in a CDW or superconductivity at low temperatures [18,23,61,62]. The transport measurements of the as-synthesized Pt_xTaSe_2 ($x = 0.05, 0.1,$ and 0.2) crystals at low temperatures were carried out to explore their exotic electronic properties. Figure 4(a) shows the temperature-dependent resistivity plot of the doped TaSe_2 crystals, where each of the $2H\text{-Pt}_x\text{TaSe}_2$ ($x = 0.05$ and 0.1) compounds display a typical metallic, with a distinct humplike transition around ~ 100 K, indicating the presence of a charge density wave behavior. The $2H\text{-Pt}_x\text{TaSe}_2$ ($x = 0.05$ and 0.1) compounds barely superconduct. Interestingly, as demonstrated in Fig. 4(b) $4H_b\text{-Pt}_{0.2}\text{TaSe}_2$, the CDW is completely suppressed and hosts superconductivity at a transition temperature of ~ 2.7 K. To further confirm the presence of superconductivity in $4H_b\text{-Pt}_{0.2}\text{TaSe}_2$ as shown in Fig. 4(c), we measured its dc magnetic susceptibility ($4\pi\chi$) for the field-cooled (FC) and zero-field-cooled (ZFC) modes at $H_{dc} = 10$ Oe from $T = 1\text{--}10$ K. The FC mode exhibits minor susceptibility, attributed to complicated magnetic flux pinning effects. From the susceptibility plot in Fig. 4(c), an inflection occurs at 2.7 K, indicating a diamagnetic transition, a typical superconducting behavior. This can also be used to estimate the superconducting critical temperature of $4H_b\text{-Pt}_{0.2}\text{TaSe}_2$, consistent with the resistivity measurements in Fig. 4(b).

Furthermore, to gain more insight into the superconducting nature of $4H_b\text{-Pt}_{0.2}\text{TaSe}_2$, we measured resistivity around the T_c at various external magnetic fields, as shown in Fig. 4(d). It is noted that the increase in the applied external magnetic field gradually suppresses the T_c of $4H_b\text{-Pt}_{0.2}\text{TaSe}_2$, extracting the transition temperature (T) where the resistivity falls 90% for each applied magnetic field. Fitting the plotted data in Fig. 4(e) with the Ginzburg-Landau equation [63]: $H_{c1}(T) = H_{c1}(0)[1 - (\frac{T}{T_c})^2]$, we can estimate the lower critical field. We get an excellent fit on fitting with the $H_{c1} = 1.425$ T. Also, fitting the data in Fig. 4(f) to the Werthamer-Helfand-Hohenberg (WHH) [64], $H_{c2}(T) = H_{c2}(0)[\frac{(1 - (\frac{T}{T_c})^2)}{(1 + (\frac{T}{T_c})^2)}]$ Based on the single-band model. As shown in Fig. 4(f), our data are well fitted to the model with an estimated upper critical field value of $H_{c2} = 2.367$ T. From the H_{c2} of $4H_b\text{-Pt}_{0.2}\text{TaSe}_2$, the coherence length [$\xi_{GL}(0)$] can be calculated using $\xi_{GL}(0) = [\phi_o / (2\pi H_{c2}(0))]^{1/2}$, where $\phi_o = h/(2e)$ [65]. Hence, $\xi_{GL}(0) = 233$ nm. Moreover, we

evaluated the superconducting gap (Δ) of $4H_b\text{-Pt}_{0.2}\text{TaSe}_2$ using the BCS theory. The equation can be approximated as $\Delta = 1.76 k_B T_c = 3.0$ meV, consistent with a conventional BCS superconductor. As observed from the extracted superconducting properties, the $H_{c2} > H_{c1}$ and $\xi_{GL}(0) >$ than the lattice of $4H_b\text{-Pt}_{0.2}\text{TaSe}_2$. Thus, this indicates that $4H_b\text{-Pt}_{0.2}\text{TaSe}_2$ is within the strong-coupling limit and a type-II superconductor [66,67].

IV. CONCLUSION

In conclusion, we have successfully synthesized and characterized single crystals of Pt_xTaSe_2 with doping concentrations of $x = 0, 0.05, 0.1,$ and 0.2 in terms of their physical, electronic, and chemical properties. XRD showed that doping 20% Pt atoms into $2H\text{-TaSe}_2$ resulted in a structural phase modification from $2H$ to $4H_b$, with the intercalation of Pt atoms into the van der Waals spacings. Further XPS analysis investigations revealed that the chemical doping of Pt atoms into TaSe_2 resulted in an injection of electrons into the system. The superconductivity of $4H_b\text{-Pt}_{0.2}\text{TaSe}_2$ was particularly enhanced, to a transition temperature of ~ 2.7 K and complete suppression of the CDW ordering state. Our findings indicate that electron doping in TaSe_2 can result in structural and electronic states modulation, which can facilitate the mediation of exotic quantum states.

ACKNOWLEDGMENTS

M.L.A. acknowledges the China postdoctoral foundation for the postdoctoral fellowship, Chinese Academy of Sciences and Bayero University, Kano. The National Synchrotron Radiation Laboratory of China, Hefei, People's Republic of China, is also acknowledged for the sample's characterizations. Also, we sincerely thank Professor Li Song of University of Science and Technology of China and his laboratory for giving us the platform to carry out the cryogenic transport experiments. Finally, I.B.G. acknowledges the PTDF Fund.

M.L.A. conceived the idea and carried out the experiments and calculations; M.L.A. and A.A.S. supervised the project; M.L.A., I.B.G., A.A.B., A.A.S., S.M.G., and F.L.A. analyzed the results and prepared the draft and final copy. All the authors participated in discussing the results, analysis, and revision of the final manuscript.

The authors declare no competing interests, either financial or otherwise.

- [1] H. Tan, Y. Liu, Z. Wang, and B. Yan, Charge Density Waves and Electronic Properties of Superconducting Kagome Metals, *Phys. Rev. Lett.* **127**, 046401 (2021).
- [2] P. Dreher *et al.*, Proximity effects on the charge density wave order and superconductivity in single-layer NbSe_2 , *ACS Nano* **15**, 19430 (2021).
- [3] Y. Wu, H. Xing, C.-S. Lian, H. Lian, J. He, W. Duan, J. Liu, Z. Mao, and Y. Liu, Ion intercalation engineering of electronic properties of two-dimensional crystals of $2H\text{-TaSe}_2$, *Phys. Rev. Mater.* **3**, 104003 (2019).

- [4] J.-H. Lee and Y.-W. Son, Gate-tunable superconductivity and charge-density wave in monolayer $1T'\text{-MoTe}_2$ and $1T'\text{-WTe}_2$, *Phys. Chem. Chem. Phys.* **23**, 17279 (2021).
- [5] A. Achari *et al.*, Alternating superconducting and charge density wave monolayers within bulk $6R\text{-TaS}_2$, *Nano Lett.* **22**, 6268 (2022).
- [6] F. H. Yu, D. H. Ma, W. Z. Zhuo, S. Q. Liu, X. K. Wen, B. Lei, J. J. Ying, and X. H. Chen, Unusual competition of superconductivity and charge-density-wave state in a compressed topological kagome metal, *Nat. Commun.* **12**, 3645 (2021).

- [7] M. Leroux, V. Mishra, C. Opagiste, P. Rodiere, A. Kayani, W.-K. Kwok, and U. Welp, Charge density wave and superconductivity competition in $\text{Lu}_5\text{Ir}_4\text{Si}_{10}$: A proton irradiation study, *Phys. Rev. B* **102**, 094519 (2020).
- [8] J.-G. Si, W.-J. Lu, Y.-P. Sun, P.-F. Liu, and B.-T. Wang, Charge density wave and pressure-dependent superconductivity in the Kagome metal CsV_3Sb_5 : A first-principles study, *Phys. Rev. B* **105**, 024517 (2022).
- [9] M. L. Adam, Z. Liu, O. A. Moses, X. Wu, and L. Song, Superconducting properties and topological nodal lines features in centrosymmetric $\text{Sn}_{0.5}\text{TaSe}_2$, *Nano Res.* **14**, 2613 (2021).
- [10] M. L. Adam and A. A. Bala, Superconductivity in quasi-2D InTaX_2 ($X = \text{S}, \text{Se}$) type-II Weyl semimetals, *J. Phys. Condens. Matter* **33**, 225502 (2021).
- [11] P. Rosenzweig, H. Karakachian, S. Link, K. Muller, and U. Starke, Tuning the doping level of graphene in the vicinity of the van Hove singularity via ytterbium intercalation, *Phys. Rev. B* **100**, 035445 (2019).
- [12] X. Liu, X. Huang, P. Song, C. Wang, L. Zhang, P. Lv, L. Liu, W. Zhang, J.-H. Cho, and Y. Jia, Strong electron-phonon coupling superconductivity in compressed $A - \text{MoB}_2$ induced by double van Hove singularities, *Phys. Rev. B* **106**, 064507 (2022).
- [13] W. Sano, T. Koretsune, T. Tadano, R. Akashi, and R. Arita, Effect of Van Hove singularities on high- T_c superconductivity in H_3S , *Phys. Rev. B* **93**, 094525 (2016).
- [14] T.-T. Gai, P.-J. Guo, H.-C. Yang, Y. Gao, M. Gao, and Z.-Y. Lu, Van Hove singularity induced phonon-mediated superconductivity above 77 K in hole-doped SrB_3C_3 , *Phys. Rev. B* **105**, 224514 (2022).
- [15] Y. Wang, J.-G. Liu, W.-S. Wang, and Q.-H. Wang, Electronic order near the type-II van Hove singularity in BC_3 , *Phys. Rev. B* **97**, 174513 (2018).
- [16] Y. Yang, L. Jia, D. Wang, and J. Zhou, Advanced strategies in synthesis of two-dimensional materials with different compositions and phases, *Small Methods* 2201585 (2023).
- [17] Z. Li *et al.*, Observation of van Hove singularities in twisted silicene multilayers, *ACS Cent. Sci.* **2**, 517 (2016).
- [18] N. F. Q. Yuan, H. Isobe, and L. Fu, Magic of high-order van Hove singularity, *Nat. Commun.* **10**, 5769 (2019).
- [19] R. Mori, P. B. Marshall, K. Ahadi, J. D. Denlinger, S. Stemmer, and A. Lanzara, Controlling a Van Hove singularity and fermi surface topology at a complex oxide heterostructure interface, *Nat. Commun.* **10**, 5534 (2019).
- [20] W. Metzner, D. Rohe, and S. Andergassen, Soft Fermi Surfaces and Breakdown of Fermi-Liquid Behavior, *Phys. Rev. Lett.* **91**, 066402 (2003).
- [21] M. D. Johannes, I. I. Mazin, and C. A. Howells, Fermi-surface nesting and the origin of the charge-density wave in NbSe_2 , *Phys. Rev. B* **73**, 205102 (2006).
- [22] D. A. Tompsett, Electronic structure and phonon instabilities in the vicinity of the quantum phase transition and superconductivity of $(\text{Sr}, \text{Ca})_3\text{Ir}_4\text{Sn}_{13}$, *Phys. Rev. B* **89**, 075117 (2014).
- [23] K. Kim, S. Kim, J. S. Kim, H. Kim, J.-H. Park, and B. I. Min, Importance of the van Hove singularity in superconducting PdTe_2 , *Phys. Rev. B* **97**, 165102 (2018).
- [24] S. Cho, H. Ma, W. Xia, Y. Yang, Z. Liu, Z. Huang *et al.*, Emergence of New van Hove Singularities in the Charge Density Wave State of a Topological Kagome Metal RbV_3Sb_5 , *Phys. Rev. Lett.* **127**, 236401 (2021).
- [25] M. Kang *et al.*, Twofold van Hove singularity and origin of charge order in topological Kagome superconductor CsV_3Sb_5 , *Nat. Phys.* **18**, 301 (2022).
- [26] D. Makogon, R. van Gelderen, R. Roldán, and C. M. Smith, Spin-density-wave instability in graphene doped near the van Hove singularity, *Phys. Rev. B* **84**, 125404 (2011).
- [27] D. I. Indolese, R. Delagrangé, P. Makk, J. R. Wallbank, K. Wanatabe, T. Taniguchi, and C. Schönberger, Signatures of van Hove Singularities Probed by the Supercurrent in a Graphene-HBN Superlattice, *Phys. Rev. Lett.* **121**, 137701 (2018).
- [28] T. Qian *et al.*, Structural phase transition associated with van Hove singularity in 5d transition metal compound IrTe_2 , *New J. Phys.* **16**, 123038 (2014).
- [29] E. A. Stepanov, V. Harkov, M. Rösner, A. I. Lichtenstein, M. I. Katsnelson, and A. N. Rudenko, Coexisting charge density wave and ferromagnetic instabilities in monolayer InSe , *npj Comput. Mater.* **8**, 118 (2022).
- [30] J. L. McChesney, A. Bostwick, T. Ohta, T. Seyller, K. Horn, J. González, and E. Rotenberg, Extended van Hove Singularity and Superconducting Instability in Doped Graphene, *Phys. Rev. Lett.* **104**, 136803 (2010).
- [31] H. LaBollita and A. S. Botana, Tuning the Van Hove singularities in AV_3Sb_5 ($A = \text{K}, \text{Rb}, \text{Cs}$) via pressure and doping, *Phys. Rev. B* **104**, 205129 (2021).
- [32] J. Bok and J. Bouvier, Superconductivity and the Van Hove scenario, *J. Supercond. Nov. Magn.* **25**, 657 (2012).
- [33] M. Uldemolins, A. Mesáros, and P. Simon, Effect of Van Hove singularities on Shiba states in two-dimensional s-wave superconductors, *Phys. Rev. B* **103**, 214514 (2021).
- [34] L. van Hove, The occurrence of singularities in the elastic frequency distribution of a crystal, *Phys. Rev.* **89**, 1189 (1953).
- [35] J. Feng *et al.*, Superconductivity induced by Lifshitz transition in pristine SnS_2 under high pressure, *J. Phys. Chem. Lett.* **13**, 9404 (2022).
- [36] M. Krottenmüller *et al.*, Indications for Lifshitz transitions in the nodal-line semimetal ZrSiTe induced by interlayer interaction, *Phys. Rev. B* **101**, 081108(R) (2020).
- [37] M. L. Adam, H. Zhu, Z. Liu, S. Cui, P. Zhang, Y. Liu, G. Zhang, X. Wu, Z. Sun, and L. Song, Charge density wave phase suppression in $1\text{T}-\text{TiSe}_2$ through Sn intercalation, *Nano Res.* **15**, 2643 (2022).
- [38] M. L. Adam and A. A. Bala, Prediction of phonon-mediated superconductivity and charge density wave in charge doped $1\text{T}-\text{HfTe}_2$, *Comput. Condens. Matter* **26**, e00527 (2021).
- [39] D. C. Miller, S. D. Mahanti, and P. M. Duxbury, Charge density wave states in tantalum dichalcogenides, *Phys. Rev. B* **97**, 045133 (2018).
- [40] L. Liu, C. Wang, L. Zhang, C. Liu, C. Niu, Z. Zeng, D. Ma, and Y. Jia, Surface Van Hove singularity enabled efficient catalysis in low-dimensional systems: CO oxidation and hydrogen evolution reactions, *J. Phys. Chem. Lett.* **13**, 740 (2022).
- [41] K. Rossnagel and N. V. Smith, Spin-orbit splitting, Fermi surface topology, and charge-density-wave gapping in $2\text{H}-\text{TaSe}_2$, *Phys. Rev. B* **76**, 073102 (2007).
- [42] S. V. Borisenko, A. A. Kordyuk, V. B. Zabolotnyy, D. V. Evtushinsky, T. K. Kim, B. Büchner, A. N. Yaresko, V. D. Borisenko, and H. Berger, Van Hove singularity as a possible origin of the bandwidth renormalization in layered superconductors, *J. Phys. Chem. Solids* **72**, 562 (2011).

- [43] V. Petkov, J. Yang, S. Shastri, and Y. Ren, Hierarchy among the crystal lattice, charge density wave, and superconducting orders in transition metal dichalcogenides, *Phys. Rev. B* **102**, 134119 (2020).
- [44] P. Giannozzi *et al.*, QUANTUM ESPRESSO: A modular and open-source software project for quantum simulations of materials, *J. Phys.: Condens. Matter* **21**, 395502 (2009).
- [45] J. P. Perdew, K. Burke, and M. Ernzerhof, Generalized Gradient Approximation Made Simple, *Phys. Rev. Lett.* **77**, 3865 (1996).
- [46] G. Pizzi *et al.*, Wannier90 as a community code: New features and applications, *J. Phys.: Condens. Matter* **32**, 165902 (2020).
- [47] M. P. L. Sancho, J. M. L. Sancho, J. M. L. Sancho, and J. Rubio, Highly convergent schemes for the calculation of bulk and surface Green functions, *J. Phys. F Met. Phys.* **15**, 851 (1985).
- [48] B. H. Toby and R. B. von Dreele, GSAS-II: The genesis of a modern open-source all purpose crystallography software package, *J. Appl. Crystallogr.* **46**, 544 (2013).
- [49] H. Luo *et al.*, Differences in chemical doping matter: Superconductivity in Ti1-xTaxSe_2 but not in Ti1-xNbxSe_2 , *Chem. Mater.* **28**, 1927 (2016).
- [50] H.-S. Tsai *et al.*, Direct synthesis of large-scale multilayer TaSe_2 on SiO_2/Si using ion beam technology, *ACS Omega* **4**, 17536 (2019).
- [51] S. Oh, S. Back, W. H. Doh, S. Y. Moon, J. Kim, Y. Jung, and J. Y. Park, Probing surface oxide formations on SiO_2 -supported platinum nanocatalysts under CO oxidation, *RSC Adv.* **7**, 45003 (2017).
- [52] Md. A. Matin, E. Lee, H. Kim, W.-S. Yoon, and Y.-U. Kwon, Rational syntheses of core-shell $\text{Fe}@\text{(PtRu)}$ nanoparticle electrocatalysts for the methanol oxidation reaction with complete suppression of CO-Poisoning and highly enhanced activity, *J. Mater. Chem. A Mater.* **3**, 17154 (2015).
- [53] T. Valla, A. V. Fedorov, P. D. Johnson, J. Xue, K. E. Smith, and F. J. DiSalvo, Charge-Density-Wave-Induced Modifications to the Quasiparticle Self-Energy in $2H-\text{TaSe}_2$, *Phys. Rev. Lett.* **85**, 4759 (2000).
- [54] A. Chikina, A. Fedorov, D. Bhoi, V. Voroshnin, E. Haubold, Y. Kushnirenko, K. H. Kim, and S. Borisenko, Turning charge-density waves into cooper pairs, *npj Quantum Mater.* **5**, 22 (2020).
- [55] P. Cudazzo, M. Gatti, and A. Rubio, Plasmon dispersion in layered transition-metal dichalcogenides, *Phys. Rev. B* **86**, 075121 (2012).
- [56] K. Rossnagel, E. Rotenberg, H. Koh, N. v. Smith, and L. Kipp, Fermi surface, charge-density-wave gap, and kinks in $2H-\text{TaSe}_2$, *Phys. Rev. B* **72**, 121103(R) (2005).
- [57] J. A. Wilson, Charge-density waves in the $2H-\text{TaSe}_2$ family: Action on the Fermi surface, *Phys. Rev. B* **15**, 5748 (1977).
- [58] H. Ryu *et al.*, Persistent charge-density-wave order in single-layer TaSe_2 , *Nano Lett.* **18**, 689 (2018).
- [59] D. S. Inosov, V. B. Zabolotnyy, D. v Evtushinsky, A. A. Kordyuk, B. Büchner, R. Follath, H. Berger, and S. V. Borisenko, Fermi surface nesting in several transition metal dichalcogenides, *New J. Phys.* **10**, 125027 (2008).
- [60] K. Lee *et al.*, Metal-to-insulator transition in Pt-doped TiSe_2 driven by emergent network of narrow transport channels, *npj Quantum Mater.* **6**, 8 (2021).
- [61] H. Isobe, N. F. Q. Yuan, and L. Fu, Unconventional Superconductivity and Density Waves in Twisted Bilayer Graphene, *Phys. Rev. X* **8**, 041041 (2018).
- [62] J. G. Storey, J. L. Tallon, and G. V. M. Williams, Saddle-point van Hove singularity and the phase diagram of high- T_c cuprates, *Phys. Rev. B* **76**, 174522 (2007).
- [63] W. H. Kleiner, L. M. Roth, and S. H. Autler, Bulk solution of Ginzburg-Landau equations for type II superconductors: Upper critical field region, *Phys. Rev.* **133**, A1226 (1964).
- [64] S. J. Williamson, Bulk upper critical field of clean type-II superconductors: V and Nb, *Phys. Rev. B* **2**, 3545 (1970).
- [65] B. Rosenstein and D. Li, Ginzburg-landau theory of Type II superconductors in magnetic field, *Rev. Mod. Phys.* **82**, 109 (2010).
- [66] J. J. Quinn and K.-S. Yi, *Solid State Physics* (Springer International Publishing, Cham, 2018).
- [67] J. Rammer, Lower critical field and magnetization of strong-coupling, type II superconductors in the dirty limit, *J. Low Temp. Phys.* **71**, 323 (1988).